

Intensity correlation in quasielastic light scattering

S. P. Kulik, A. N. Penin, P. A. Prudkovskii, and M. V. Chekhova

M. V. Lomonosov State University, 119899 Moscow, Russia

(Submitted 17 May 1996)

Zh. Éksp. Teor. Fiz. **110**, 1712–1726 (November 1996)

The correlation of the intensity is investigated for light scattered by a traveling acoustic wave with coherent or quasithermal statistics, depending on the excitation conditions. It is shown that the correlation of the scattered light intensity mirrors the statistics of the scattering acoustic wave. In the case of scattering by quasithermal sound prominent features not apparent in the angular profile of the scattering line are observed in the angular dependence of the intensity correlation function. The fourth-order interference pattern with respect to the field is observed for two independent, quasithermal light sources. © 1996 American Institute of Physics. [S1063-7761(96)01111-0]

1. INTRODUCTION

The problems traditionally solved by scattered light spectroscopy generally fall within the category of inverse problems: A conclusion as to certain properties of a scattering medium can be drawn by measuring the parameters at the output for known parameters of exciting (or sensing) radiation at the input. The same applies in every respect to optical mixing spectroscopy, where the functional relationship between the statistical properties of a scattering field and medium is analyzed.¹ Complete statistical information about a random field is embodied in the set of moments of all orders, but practical efforts are usually limited to the first two even moments. An exception is found in the extensive class of randomly inhomogeneous media with Gaussian statistics, where the higher moments of the field leaving the medium are expressed in terms of the lowest moments.

On the other hand, an urgent problem is encountered in the search for new sources of nontrivial optical fields and fields with restructurable statistics. The idea here is that the desired result is obtainable specifically from light scattering processes (elastic as well as inelastic). For example, when the frequency shift is decreased (or the effective temperature is increased) in spontaneous Raman scattering, the bunching parameter $g^{(2)}$ of the scattered light in the limit varies from ∞ ($h\omega > kT$) to 2 ($h\omega < kT$).² Another example can be found in the influence of anharmonicity of phononlike elementary excitations in both the equilibrium and the excited state on the statistics of scattered light.³ Also a topic of discussion is the nonclassical nature of the fields in the separate detection of the photon and phonon “components” in polariton scattering.^{4,5}

In this regard the problem to be solved in light scattering spectroscopy can be restated as follows: to specify the statistical properties of the medium in such a way that the distribution of the moments of the scattered field will exhibit nontrivial features.

In the present article we discuss the results of experiments on light scattering by a quasithermal source in the form of a traveling elastic wave modulated by narrowband Gaussian noise. We have investigated the statistical proper-

ties of the scattered light using intensity fluctuation spectroscopy. We have shown that:

- 1) an effective source of directional quasithermal radiation having a high luminance and an adjustable coherence length can be created by an acoustooptic interaction technique;
- 2) the angular dependence of the second moment of the intensity can reveal prominent features not manifested in the first-order line profile;
- 3) the two-photon interference effect discussed in quantum optics has a classical analog.

The article is organized as follows. The experimental arrangement is shown schematically in Sec. 2, along with various modifications. A group of experiments to study the correlation of the intensity in scattering by coherent and quasithermal sounds is described. In Sec. 3 the data from all the experiments are analyzed and compared with the results of calculations. Finally, the study is summarized in Sec. 5.

2. EXPERIMENTAL

In intensity fluctuation spectroscopy a Brown–Twiss interferometer is traditionally used to separate the contributions of spatial modes.⁶ Together with this system we used a second arrangement based on the correlation of the Stokes (s) and anti-Stokes (a) fields in dual-beam pumping:

$$\mathbf{k}_{L1} + \mathbf{k}_{L2} = \mathbf{k}_s + \mathbf{k}_a,$$

where \mathbf{k}_{L1} and \mathbf{k}_{L2} are the incident wave vectors, and \mathbf{k}_s and \mathbf{k}_a are the scattered Stokes and anti-Stokes wave vectors. Correlation arises in the classical description of light scattering by fluctuations of the permittivity $\varepsilon = \langle \varepsilon \rangle + \Delta \varepsilon$, where the intensity fluctuations in \mathbf{k}_s and \mathbf{k}_a modes are synchronized by virtue of the total real Fourier component $\Delta \varepsilon_q = (\Delta \varepsilon_{-q})^*$, where \mathbf{q} is the scattering vector.⁷ We note that condition (1) can also be satisfied for modes of different frequencies. From the standpoint of investigating the correlation of intensities in quasielastic scattering, the dual-beam pump configuration is described by the same mathematical model as the Brown–Twiss interferometer configuration (see Sec. 3). In our work some of the measurements were performed using both configurations, and some using only one

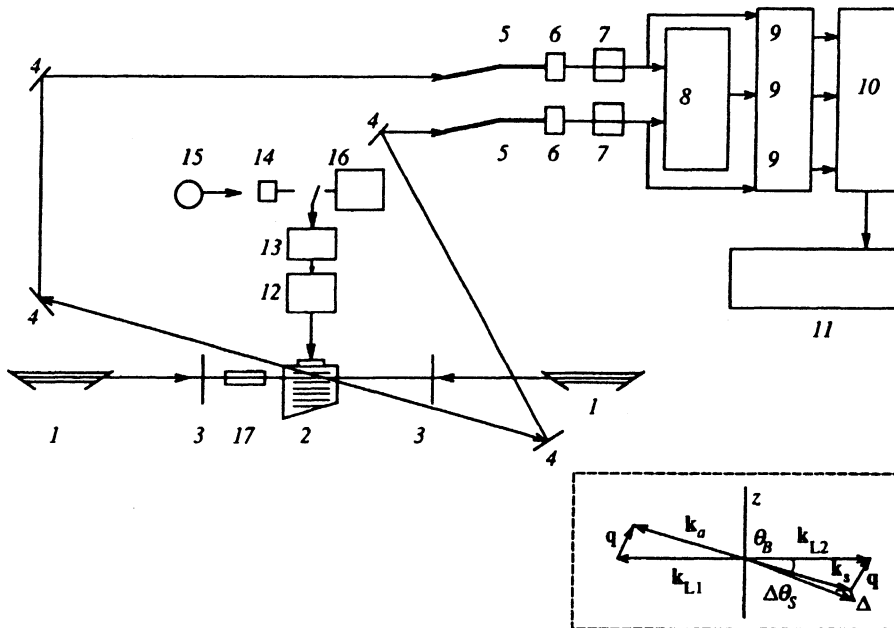


FIG. 1. Experimental arrangement. 1) He-Ne lasers; 2) acoustooptic cell; 3) diaphragms; 4) rotatable mirrors; 5) scannable optical fibers; 6) photomultipliers (type FEU-79); 7) amplifier-discriminators; 8) coincidence circuit; 9) counters; 10) CAM-AC module; 11) PC/AT 386 computer; 12) filter for the electrical signal; 13) wide-band amplifier; 14) photomultiplier; 15) stabilized optical fiber; 16) oscillator; 17) plane-parallel plate. Inset: orientation of the wave vectors for Bragg synchronism: \mathbf{k} denotes the light wave vectors; \mathbf{q} is the ultrasonic wave vector; $\Delta\theta_S$ and Δ are the angular and wavenumber deviations; θ^V is the Bragg angle; z is the direction of parallel displacement of one of the pump beams.

of them. When referring to each experiment below, we shall make special note of which configuration has been used for the measurements.

Figure 1 shows the experimental arrangement with oppositely directed beams. A single-mode He-Ne laser beam (coherence length $l_{\text{coh}} \sim 14$ m, divergence $\Delta\theta \sim 10^{-3}$ rad) was directed into an acoustooptic cell through an iris diaphragm used to define the diameter of the beam. Elastic waves were generated in a fused quartz sample by the following procedure.

Pulses from a photomultiplier ($\tau_{\text{pulse}} < 10$ ns) illuminated by radiation from a stabilized light-emitting diode were sent through a wideband amplifier to an active filter with a bandwidth $\Delta f \sim 2-8$ MHz and center frequency $\Omega = 50$ MHz. The spectrum of the electrical signal was monitored by means of a spectrum analyzer. Since the spectrum of the signal sent to the filter far exceeded the filter bandwidth ($\Delta\Omega \gg \Delta f$), the intensity fluctuations at the filter output were normalized.⁸ The resulting signal, representing narrowband ($\Omega \gg \Delta f$) Gaussian noise, excited from the surface a traveling acoustic wave in the fused quartz sample. To avoid the formation of a standing wave by reflection, the opposite face of the sample was beveled at a 30° angle relative to the acoustic wavefront. An elastic wave thus propagated in the cell, generating periodic perturbations of the permittivity ε through the elastooptic effect:

$$\varepsilon = \langle \varepsilon \rangle + \Delta\varepsilon,$$

where

$$\langle \varepsilon \rangle = n^2, \quad \Delta\varepsilon = A(t, z) \exp\{-i\Omega t + iqz\},$$

$A(t, z)$ is the complex amplitude of the Gaussian stochastic process, $q = \Omega/v$, and v is the sound velocity. We refer to this technique of acoustic wave generation as the quasithermal method.

We also used an amplitude-stabilized narrowband ($\Delta f < 10$ kHz, $\Omega = 50$ MHz) signal generator as the source of elastic waves. The perturbations of the permittivity had a harmonic form in this case:

$$\Delta\varepsilon = A \exp\{-i\Omega t + iqz + i\varphi(t)\}, \quad A = \text{const},$$

creating a coherent regime. The length of the zone of interaction between light and sound was determined by the width of the acoustic column l_{sound} (of order two centimeters) and the diameter of the laser beams (from 0.8 mm to 3 mm). In both ultrasound generating techniques a regime closely resembling Bragg diffraction was established, with the wave parameter $Q = q^2 l_{\text{sound}} / 2\pi k > 1$ (k and q are the wave vectors of light and sound). In directions satisfying the phase-locking conditions we have

$$\mathbf{k}_a = \mathbf{k}_{L1} + \mathbf{q}, \quad \mathbf{k}_s = \mathbf{k}_{L2} - \mathbf{q}.$$

The differently directed beams with frequencies $\omega_s = \omega_0 - \Omega$ and $\omega_a = \omega_0 + \Omega$ diffracted by the periodic perturbation of the permittivity (Fig. 1) were directed into an optical intensity correlator by means of an optical fiber. (In the Brown-Twiss configuration a single beam was used instead of two oppositely directed beams, but after the acoustooptic cell the scattered beam was separated by a beam splitter into two parts, which were then directed to photomultipliers 1 and 2). The correlator consisted of two photomultipliers (type FEU-79) operating in the photon-counting mode, their output pulses being sent to a coincidence circuit and counters after preamplification and discrimination. The measurement results consisted of the photon counts N_1 and N_2 , averaged over the time interval T , which were proportional to the intensities $I_1 \approx I_s$ and $I_2 \approx I_a$, respectively (in the Stokes and anti-Stokes channels), along with the number of coincidences of photon detections N_3 , which is proportional to the second-order intensity correlation function

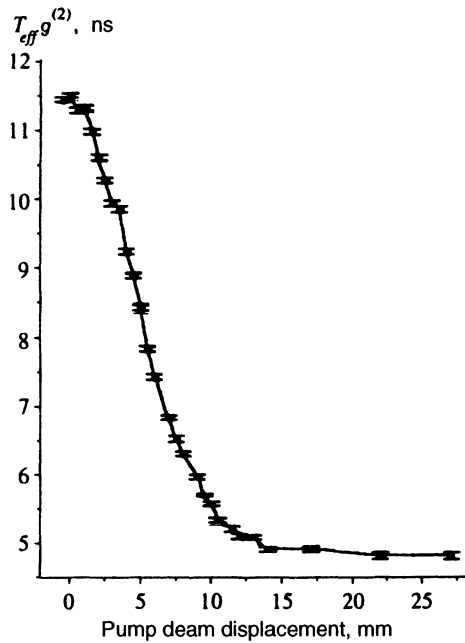


FIG. 2. Intensity correlation function vs displacement of one of the pump beams along the vector \mathbf{q} .

$G^{(2)}$. After statistical processing, the normalized intensities $I^{\text{norm}} = I_s / I_a$ and the correlation function were calculated:

$$g^{(2)} = \frac{N_3}{N_1 N_2 T_{\text{eff}}} = \frac{\langle I_s I_a \rangle}{\langle I_s \rangle \langle I_a \rangle},$$

where T_{eff} is the effective firing time of the coincidence circuit, which varied over the range $5.5 \text{ ns} < T_{\text{eff}} < 8 \text{ ns}$ in our experiments.

Figure 2 shows the normalized correlation function $g^{(2)} T_{\text{eff}} = N_3 / N_1 N_2$ as a function of the parallel displacement of one of the pump beams relative to the other along the vector \mathbf{q} (since the light frequencies ω_i are much higher than the acoustic frequency Ω , where $i = L, a, s$, the wave vectors \mathbf{k}_i are almost perpendicular to \mathbf{q}). Ultrasound was generated in the quasithermal regime. The experiment was carried out using the dual-beam pump configuration. Beam shifting was achieved by rotating the plane-parallel plate 17 (Fig. 1) inserted into the first beam. When the axes ($z=0$) of the opposed pump beams \mathbf{k}_{L1} and \mathbf{k}_{L2} are exactly aligned, the function $g^{(2)}$ assumes the value 2 ($T_{\text{eff}} = 5.5 \text{ ns}$). As the beam shift is increased, the correlation function decreases and asymptotically approaches unity. In the coherent regime $g^{(2)}$ is independent of the coordinate z and coincides with the level obtained in calibration measurements, $g^{(2)} = 1$. In the experiments discussed here, the pump beams had a diameter $D = 3 \text{ mm}$, the width of the spectrum of the ultrasound-generating electrical signal was $\Delta f \cong 7 \text{ MHz}$, the distance from the cell to the photomultiplier was $l \cong 5 \text{ m}$, and the diameter of the optical fiber was $400 \mu\text{m}$.

Figure 3 shows $g^{(2)} T_{\text{eff}}$ (b, d) and I^{norm} (a, c) as functions of the scattering angle in the Stokes channel (for a fixed position of the optical fiber in the anti-Stokes channel) for the quasithermal generation regime. It is readily shown that

the deviation of the scattering angle $\Delta\theta$ from the Bragg angle is proportional to the departure of the wave vector from Bragg synchronism:

$$\Delta\mathbf{k} = \mathbf{k}_L - \mathbf{k}_s - \mathbf{q}.$$

The graphs in Fig. 3 actually represent the directional profiles of the first-order $[I(\Delta\mathbf{k})]$ and second-order $[g^{(2)} \times (\Delta\mathbf{k}) T_{\text{eff}}]$ intensity scattering lines. The parameter is the diameter D of the pump beams, which was set by means of diaphragms: $D = 0.8, 1.5, 2., 2.5, 3 \text{ mm}$. The diameter of the optical fibers was $200 \mu\text{m}$, and the effective time was $T_{\text{eff}} = 8 \text{ ns}$.

Characteristically, as the beam diameter is increased, the angular dependence of the correlation function $g^{(2)}(\Delta\theta)$ acquires additional maxima, whose repetition period decreases as D is increased. At a certain value of D (3 mm) the individual maxima begin to overlap and cannot be resolved by the receiving system. The angular distributions of I^{norm} do not exhibit oscillatory behavior. For the coherent regime, within the measurement error limits (2%), $g^{(2)}(\Delta\theta)$ coincides with unity, independently of the position of the optical fiber.

These graphs were obtained using the Brown–Twiss configuration with single-beam pumping and a splitter mirror.

Figure 4 shows the schematic arrangement used to observe light interference from two independent thermal sources. Two parallel, unidirectional He–Ne laser beams are diffracted by an ultrasonic wave. For a sufficient distance from the cell to the splitter mirror the diffracted beams overlap as a result of divergence, so that each photodetector records the light contribution from both acousto-optic interaction zones. The scattered light is directed onto two photodetectors by means of a beam splitter (Brown–Twiss configuration). Figure 5 shows the spatial variations of $I^{\text{norm}}(\Delta\theta)$ (a) and $g^{(2)}(\Delta\theta) T_{\text{eff}}$ (b) obtained when the cross section of the overlapping beams is scanned by the optical fiber of the first channel. The distance between the pump beams was $l = 8 \text{ mm}$ and exceeded the coherence length of the ultrasonic beam. The distance between the maxima of the correlation function diminished as l was increased.

3. DISCUSSION

3.1. Narrowband Source of a High-Luminance, Quasithermal Field

It is readily verified that the scattered (or diffracted) light has Gaussian statistics for the chosen method of ultrasonic wave generation. Indeed, the source of elastic waves in the cell is an electrical signal in the form of narrowband Gaussian noise operating in the plane $z=0$. One of the possible representations of this type of process has the form

$$A = A(t) \exp[-i\Omega t],$$

where $A(t)$ is the complex random amplitude. The permittivity at an arbitrary point z varies according to the law

$$\varepsilon = \Delta\varepsilon(z, t) \exp[-i(\Omega t - qz)] + \langle \varepsilon \rangle,$$

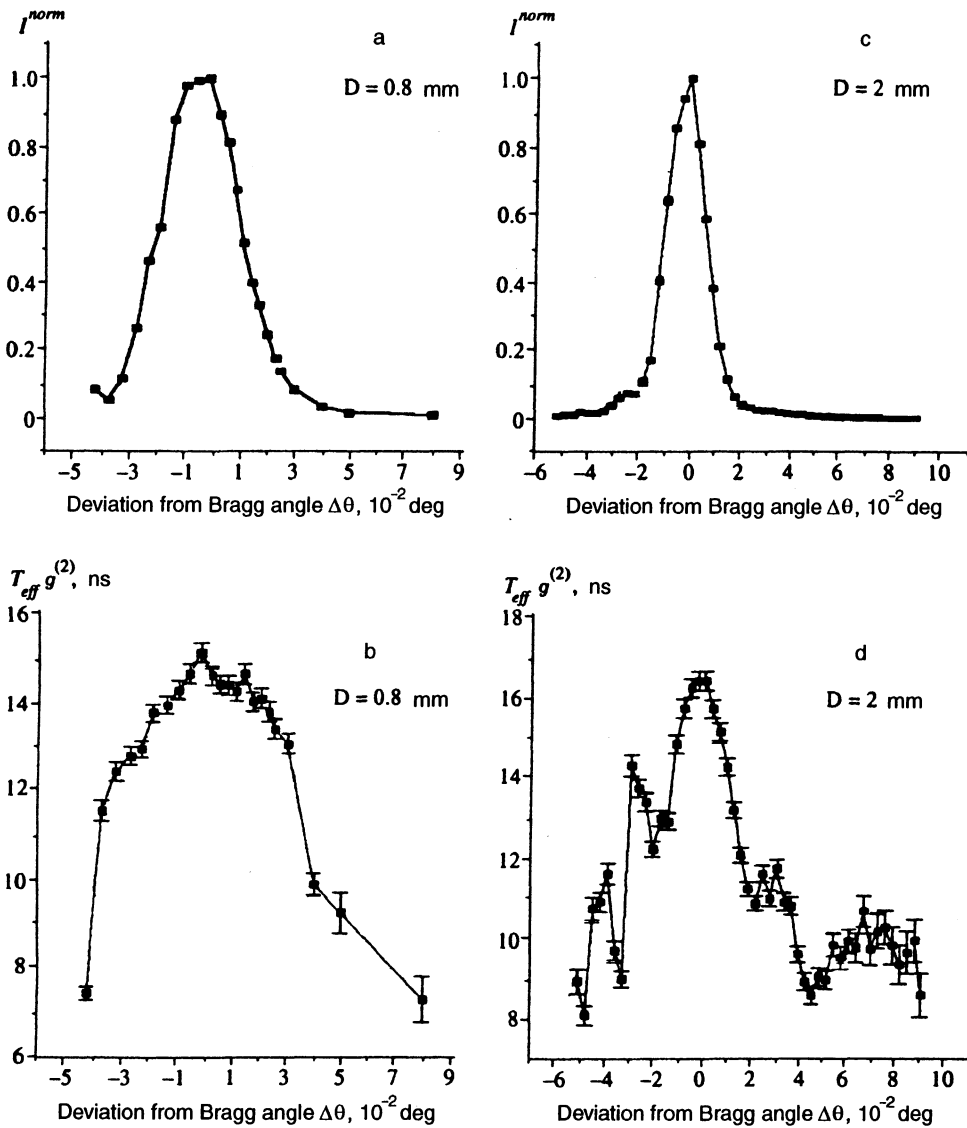


FIG. 3. Angular profiles of the normalized intensity (a, c) and the correlation function (b, d). a, b) Diameter of pump beam 0.8 mm; c, d) 2 mm.

and the amplitude $\Delta\varepsilon(z, t)$ is related to the complex signal amplitude in the plane $z_0=0$ by the equation

$$\Delta\varepsilon(z, t) = \eta A(z=0, t - z/v), \quad (1)$$

where v is the sound velocity, and η is a constant determined by the elements of the piezoelectric and elasto-optic tensors. Consequently, the fluctuations of ε at each point of the acousto-optic cells are described by the function $A(t)$ and are therefore essentially Gaussian. The fluctuations at two points z_1 and z_2 can be regarded as independent if the distance $\Delta z = z_1 - z_2$ between them is greater than $z_{\text{coh}} = v/\Delta f = v\tau_{\text{coh}}$, where Δf is the half-width of the frequency spectrum of the Gaussian noise, and τ_{coh} is the ultrasound coherence time, which coincides with the reciprocal of the half-width of the spectrum of the electrical signal.

In our experiments the width of the spectrum was 5 MHz in measurements of the angular dependence of the correlation function and the intensity, and it was 2 MHz in the investigation of interference of the intensities of two independent sources. The transverse acoustic wave velocity is

$v_{\text{sound}} = 3.76 \cdot 10^5$ cm/s, so that for the coherence length we obtain $z_{\text{coh}} \sim 0.8$ mm and 1.9 mm, and for the coherence time $\tau_{\text{coh}} \sim 300$ ns and 500 ns, respectively.

The statistical properties of the diffracted laser beam depend directly on the form of the distribution of the random function $A(t)$. We examine two limiting cases. In the first the diameter of the incident beam on the cell and, hence, the transverse zone of interaction of light and sound is smaller than the coherence length: $D < z_{\text{coh}}$. The intensity of the scattered beam is then modulated by the function $A(t)$ with Gaussian statistics. Accordingly, the light has Gaussian statistics as well.¹ In the other limiting case, $D > z_{\text{coh}}$, the electromagnetic field of the scattered light contains a contribution from several independent spatial zones, each of whose fluctuations has a Gaussian character. This endows the field with thermal statistics, but it will be shown below that the fourth moment of the field has a nontrivial spatial distribution.

In coherent ultrasound generation we have $A \equiv \text{const}$,

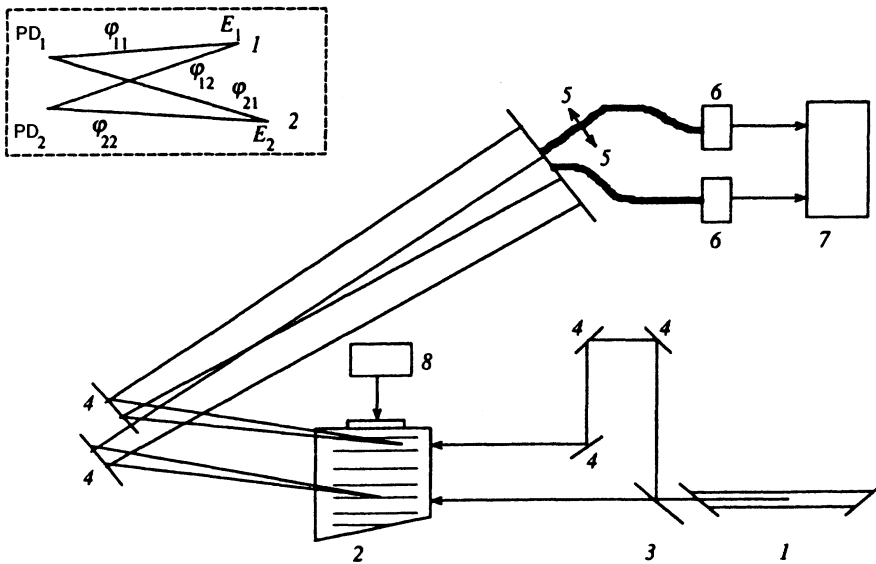


FIG. 4. Optical system for the observation of light interference from two uncorrelated scattering zones. 1) He-Ne laser; 2) acousto-optic cell; 3) semitransparent mirror; 4) rotatable mirrors; 5) scannable optical fibers; 6) photodetectors; 7) intensity correlator; 8) electrical signal source. Inset: geometry of observation of interference from two independent light sources: 1, 2) light sources; PD1, PD2) photodetectors; E_i, φ_{ij} are the strengths and regular phases of the fields ($i, j=1,2$), and L is the distance from the sources to the photodetectors.

$l_{\text{coh}} > 40$ cm, and the distribution of the scattered light statistics is Gaussian (coherent state of the field).

We note that the method used in the present study to create a light field with thermal statistics has several advantages over other known methods:

1) The radiation is highly directional. The angular divergence of the diffracted beam is determined by the minimum divergence of either the input laser beam or the acoustic beam.⁹ The problem of minimizing these factors has been solved in present-day acousto-optics and laser physics.

2) The coherence length can be varied by regulating the bandwidth of the filter used for the electrical signal.

3) The thermal radiation has a high luminance comparable with the luminance of laser sources (more than 10^{12} photons per mode).

Probably the nearest analogs of such a source of a thermal field in the optical range are a spinning matte disk illuminated by laser light¹⁰ and a multimode laser with unlocked modes.¹¹ The disadvantages of these sources are high divergence (in the first case) and a short coherence time (in the second case).

The results shown in Fig. 2 demonstrate the direct measurement of the coherence length of an ultrasonic wave from the value of the second-order intensity correlation function. Exact alignment of the axes of the opposed beams ($z=0$) corresponds to the maximum correlation function of the thermal field: $g^{(2)}=2$. The decrease in the correlation function for $z>0$ is caused by desynchronization of the intensity fluctuations of the diffracted beams \mathbf{k}_s and \mathbf{k}_a , when the scattering zones are separated by a distance greater than the coherence length z_{coh} of the ultrasonic wave. The value of the latter measured by this technique, $z_{\text{coh}}=0.47 \pm 0.04$ mm, agrees with the value calculated from the width of the spectrum (7 MHz): $z_{\text{coh}}=z/\Delta f=0.54 \pm 0.08$ mm. In diffraction by a coherent acoustic wave, on the other hand, the scattered field has the same statistics as the incident (coherent) field, while the correlation function does not depend on the z coordinate and assumes the only possible value $g^{(2)}=1$.

3.2. Angular Distributions of the Moments of the Scattered Field

A more unexpected outcome, in our opinion, is found in the results of measurements of the directional profile of the diffracted beam (Fig. 3). The angular dependence of the normalized intensity of the Stokes beam $I^{\text{norm}}(\Delta\theta)$ consists of a solitary maximum and is essentially independent of the transverse width of the interaction zone in both the coherent and the thermal regime. For certain values of D , however, the angular dependence of the correlation function exhibits nonmonotonic behavior (Fig. 3d) and has a greater half-width than the corresponding distributions of I^{norm} . The line profile of the correlation function is asymmetric, attaining a value of 2 at the maximum and decreasing by an oscillating route to the level of 1 at the edges. Slight displacements of the optical fiber in the anti-Stokes (reference) channel cause both the principal and the secondary maxima to shift and lead to distortion of the line profile. The oscillations of the correlation function show the highest contrast for $D \geq 2$ mm. For $D < z_{\text{coh}} \sim 1$ mm the correlation function does not contain any secondary maxima and, as before, remains broader than the I^{norm} distribution.

We now estimate the angular dependence of the second and fourth moments of the scattered field in the approximation of a planar specified optical pump and an essentially Gaussian acoustic wave. The scattering volume is determined by the zone of intersection of the light and sound fields. Its longitudinal dimension coincides with the width of the acoustic beam, and its transverse dimension is set by the diameter of the diaphragm D . The angular spectrum of the scattered light is calculated as a function of the deviation of the transverse wave vector from Bragg synchronism:

$$\Delta = \Delta \mathbf{k}_{\perp} = \mathbf{k}_L - \mathbf{k}_s - \mathbf{q}.$$

The strength of the scattered field is represented by the analytical signal

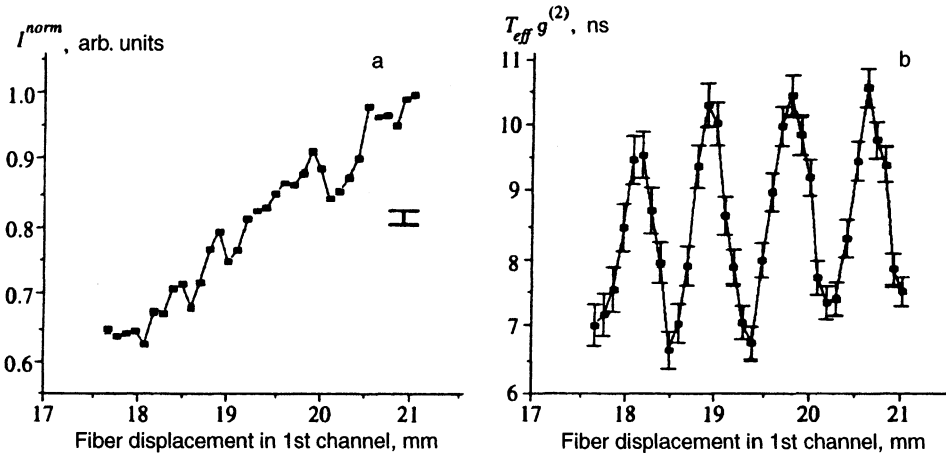


FIG. 5. Spatial (phase) dependence of the normalized intensity (a) and the correlation function (b) for two independent thermal sources.

$$E_s(t) \propto \int_{-D/2}^{+D/2} \Delta \varepsilon(z, t) \exp(i\Delta z) dz, \quad (2)$$

where all factors that do not depend on Δ and z and hence do not affect the angular profile of the line are omitted. The integration is carried out within the limits of the aperture of the pump beam, and we consider the one-dimensional case, where the pump is bounded only in the z -direction. According to Eq. (2), the permittivity fluctuations $\Delta \varepsilon(z, t)$ represent a Gaussian random function, and its instantaneous distribution $\Delta \varepsilon(z, t = \text{const})$ is specified by the distribution of the random function $A(t)$. The light intensity recorded by each photodetector is written in the form

$$I_i = \langle |E_s^i|^2 \rangle = \left\langle \int_{-D/2}^{+D/2} \Delta \varepsilon(z, t) \Delta \varepsilon^*(z', t) \times \exp\{i\Delta(z - z')\} dz dz' \right\rangle, \quad (3)$$

where the subscript $i = 1, 2$ labels the corresponding photodetector. The one-time correlation function describing the permittivity fluctuations has the form

$$B(z - z') \equiv \langle \Delta \varepsilon(z, t) \Delta \varepsilon^*(z', t) \rangle = \frac{1}{z_{\text{coh}}} \sqrt{\frac{2}{\pi}} \times \exp\left\{-\frac{(z - z')^2}{2z_{\text{coh}}^2}\right\}. \quad (5)$$

After integration, the expressions for the intensity and the correlation function of the scattered light acquire the form

$$I_i = 2 \int_0^D y B(y) (D - y) \cos(\Delta_i y) dy, \quad (5)$$

$$g^{(2)}(\Delta_1, \Delta_2) = 1 + \frac{|J_{12}|^2}{I_1 I_2}, \quad (5')$$

where

$$J_{12} = \frac{2}{\Delta} \int_0^D B(y) \left[\sin\left(\Delta_1 y + \frac{\tilde{\Delta} D}{2}\right) - \sin\left(\Delta_2 y + \frac{\tilde{\Delta} D}{2}\right) \right] dy, \quad \tilde{\Delta} \equiv \Delta_1 - \Delta_2. \quad (6)$$

The calculated distributions of $g^{(2)}$ and I^{norm} (Fig. 6) depend on the ratio between the diameter of the pump beam D and the coherence length of the acoustic wave z_{coh} . In the case $D < z_{\text{coh}}$ the fields diffracted at different points of the scattering volume interfere and produce an angular profile of the intensity line of the form $\sin c(\tilde{\Delta} D)$. On the other hand, the intensity fluctuations in the scattering volume are correlated, creating a broad angular dependence of the correlation function. Analogous curves describe the angular distribution of the correlation function of a thermal point source. As the diameter D is increased, the intensity line profile $I^{\text{norm}}(\Delta)$ loses its interference character and assumes the form of a solitary peak. However, the corresponding correlation functions oscillate considerably, even for values of $D/z_{\text{coh}} \sim 3-5$. The distance between the minima of the correlation function is approximately equal to $\Delta_m = 2\pi m/D$, where m is an integer. For $D/z_{\text{coh}} \gg 1$ the angular profile of the intensity line is determined by the coherence length of the acoustic wave z_{coh} , and the width of the correlation function is determined by the transverse width of the pump beam D .

Figure 6 shows the results of numerical calculations of the angular distributions $I^{\text{norm}}(\Delta \theta_1)$ and $g^{(2)}(\Delta \theta_1)$ for the cases $D/z_{\text{coh}} = 1$ (a, b) and $D/z_{\text{coh}} = 2.5$ (c, d). The deviation from the synchronism angle (Bragg angle) $\Delta \theta_1$ is linearly related to the frequency separation Δ_1 : $\Delta \theta_1 = \Delta_1/k_s$ (Fig. 1). We assume that the second detector records scattering exactly at the Bragg angle: $\Delta_2 = 0$ and $\tilde{\Delta} = \Delta_1$. If the second detector records scattering at an angle $\theta_2 \neq \theta^B$ (shift from the position of the intensity maximum), the profile of the correlation function becomes asymmetric and better matches the experimental curves (Fig. 3). We note that the angular dependences of the correlation function are considerably more informative than the I^{norm} distributions. Both the measured

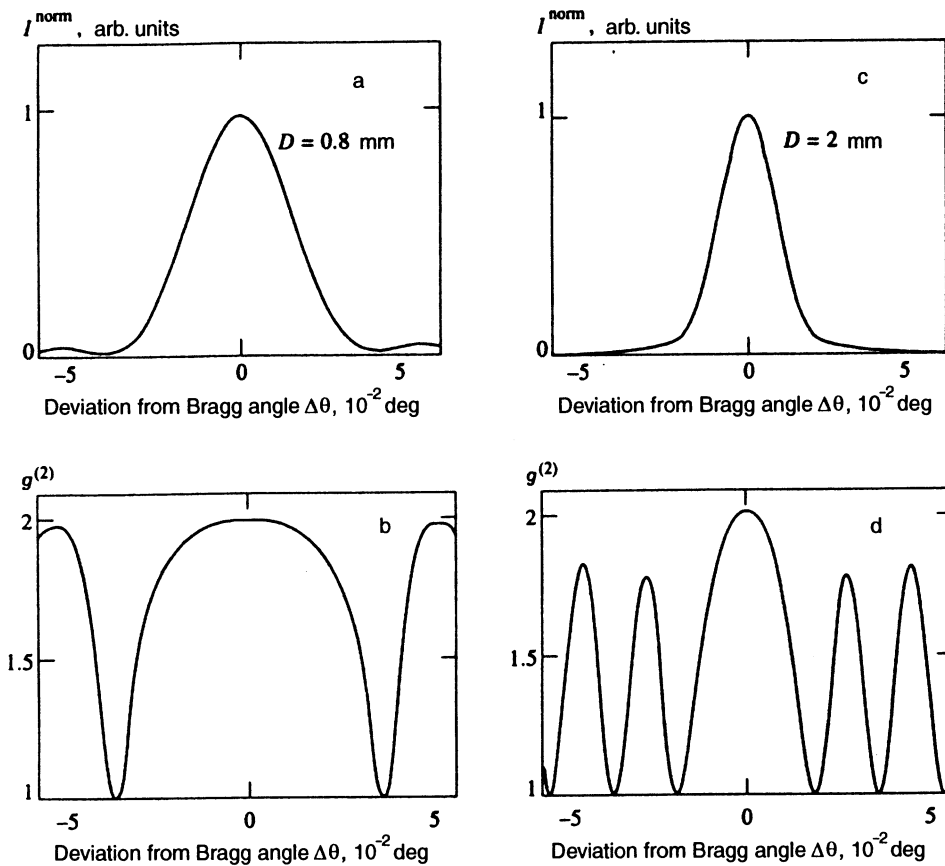


FIG. 6. Calculated angular dependence of the normalized intensity (a, c) and the correlation function (b, d). a, b) Width of the interaction zone $D = 0.8$ mm; c, d) 2 mm.

and the calculated functions $g^{(2)}(\Delta\theta)$ are broader and contain several secondary maxima, even for values of the frequency separation at which the signal intensity approaches zero asymptotically. The experimental implementation of this situation meets with well known difficulties, primarily a low signal-to-noise ratio. However, this problem can often be circumvented by measuring the second moment of the intensity, because the signal and the noise differ in nature. The investigated radiation obeys Gaussian statistics. The noise is a composite of unavoidable random external illuminations (multimode field) and instrument electronic noise, i.e., it is described by a Poisson distribution function. For a counting rate of noise pulses approximately equal to $N_n \sim \langle I_n \rangle = 150$ Hz (when the measured radiation is overlapped) the correlation function differs significantly from unity for a signal-to-noise ratio $h \sim 1/3$. Here allowance for the mixing of a signal having Gaussian statistics with noise characterized by Poisson statistics lowers the contrast of the correlation function. The corresponding correction factor used in the calculations is of the order of

$$\frac{G_{\text{source}}^{(2)} - 1}{G_{\text{meas}}^{(2)} - 1} = (1 + h^{-1})^2,$$

where G_{source} and G_{meas} are the true and measured values of the correlation function, and $h = \langle I_{\text{sig}} \rangle / \langle I_n \rangle$. The incomplete contrast of the experimental correlation functions is also attributable to inadequate spatial resolution of the receiving system. The failure to observe quantitative similarity between the analytical and experimental curves might be attrib-

utable to the use of the one-dimensional approximation, although proper estimates of the coherence length from the line profile of the correlation function corroborate the correctness of the choice of model.

3.3. Interference of Intensities from Independent Sources

We have hypothesized that the experimentally observed features of the line profile are associated with second-order interference from independent monochromatic thermal sources.^{12,13} We have assembled the apparatus shown in Fig. 4 to test this hypothesis. The role of the independence sources is filled by two scattering zones in the acousto-optic cell, which are separated by a distance greater than the coherence length of the acoustic wave, $l > z_{\text{coh}}$. The intensity fluctuations of the two diffracted beams are uncorrelated by definition in this case, hence an interference pattern (second-order in the field) is not formed. Regardless of the statistics of the field sources, the intensity of the light incident on the photodetector 1 represents the superposition of the contributions from each zone (see Fig. 4):

$$I^{(1)} = \langle (E_1 e^{i\varphi_{11}} + E_2 e^{i\varphi_{21}})(E_1^* e^{-i\varphi_{11}} + E_2^* e^{-i\varphi_{21}}) \rangle. \quad (7)$$

Here the angle brackets signify time averaging, E_1, E_2 and $\varphi_{11}, \varphi_{21}$ are (respectively) the complex amplitudes and regular phases of the random fields (e.g., $\varphi_{11} = 2\pi L/\lambda$, where L is the distance between the first source and the photomultiplier 1), and the rapidly varying frequency factors $e^{i\omega t}$ are omitted. Analogously,

$$I^{(2)} = \langle (E_1 e^{i\varphi_{22}} + E_2 e^{i\varphi_{22}})(E_1^* e^{-i\varphi_{12}} + E_2^* e^{-i\varphi_{22}}) \rangle. \quad (8)$$

Since the sources are assumed to be independent (the distance between them being greater than the coherence length of the acoustic wave), terms in odd powers of E_1 and E_2 vanish in the expression for the intensity correlation function. All that remains are terms of the form $\langle E_1^* E_1 E_2^* E_2 \rangle$ and $\langle E_1^* E_1 E_1^* E_1 \rangle$. We make use of the fact that

$$\langle E_1^* E_1 E_1^* E_1 \rangle = \langle I_1^2 \rangle, \quad \langle E_1^* E_1 E_2^* E_2 \rangle = \langle I_1 \rangle \langle I_2 \rangle$$

(the sources are independent). Setting $I_1 = I_2 = I$ for simplicity, we obtain

$$\langle I^{(1)} I^{(2)} \rangle = 2 \langle I^2 \rangle + 4 \langle I \rangle^2 \cos^2 \varphi / 2,$$

$$\varphi = \varphi_{11} - \varphi_{12} + \varphi_{22} - \varphi_{21}. \quad (9)$$

Bearing in mind that $\langle I^2 \rangle = 2 \langle I \rangle^2$ for Gaussian fields, we obtain a final expression for the normalized cross-correlation function of two independent thermal sources:

$$g^{(2)} = \frac{\langle I^{(1)} I^{(2)} \rangle}{\langle I^{(1)} \rangle \langle I^{(2)} \rangle} = \frac{\langle I^2 \rangle}{\langle I \rangle^2} = 1 + \cos^2 \varphi / 2. \quad (10)$$

It is evident from Eq. (12) that the required correlation function depends periodically on a combination of the relative phases of the scattered field, taking values from unity (at the minimum) to two (at the maximum).

The phase φ was varied experimentally by displacing the optical fiber in one detector in the transverse direction relative to the axis of propagation of the beams. The quantity $\varphi_{11} - \varphi_{12}$ was varied in this way, but the phase difference $\varphi_{22} - \varphi_{21}$ was left unchanged. We note that the distance l between the sources (e.g., stars) can be determined by measuring the phase shift between consecutive maxima (minima) of the interference pattern if the distance L to the sources is known.

Figure 5 illustrates the ‘‘two-photon’’ (or ‘‘latent’’) optical interference effect. Here the oscillating phase dependence appears in the second-order correlation function of the intensity (Fig. 5b) and is not observed in the second moment of the field (Fig. 5a) [the nonmonotonic behavior of the function $I^{\text{norm}}(x)$ is induced by the transverse inhomogeneity of the primary laser beam]. This fact does not contradict the Siegert relation, which interrelates the first- and second-order intensity correlation functions for fields with thermal statistics:⁸

$$g^{(2)}(\tau) = 1 + |g^{(1)}(\tau)|^2.$$

An example of this situation is found in the experiments of Brown and Twiss,¹⁴ who succeeded in measuring the angular diameters of stars with higher accuracy than previously achieved by the interference procedure.¹⁾

We emphasize that these remarks concern the purely classical description of the interference of classical fields. It follows from Eqs. (11) and (12) that the maximum attainable contrast of the correlation functions

$$m = \frac{g_{\max}^{(2)} - g_{\min}^{(2)}}{g_{\max}^{(2)} + g_{\min}^{(2)}}$$

for thermal and coherent fields has the values 1/3 and 1/2, respectively. Higher contrasts (theoretically up to 100%) are possible for light fields with nonclassical statistics, where oscillating phase dependences of the correlation functions have also been observed.^{15,16} However, the very occurrence of so-called latent interference for a classical thermal field invites constructive skepticism in regard to assertions about the decidedly quantum nature of this phenomenon. One final consideration is that it should be feasible to set up relatively simple optical experiments to exhibit (albeit with lower contrast) classical analogies and other effects such as ‘‘quantum image transfer’’¹⁷ and ‘‘quantum cryptography’’¹⁸ (a detailed discussion of the occurrence of quantum and classical properties of light fields can be found in a recent survey.¹⁹

4. CONCLUSION

In essence, we have investigated scattering by excited acoustic phonons with a specified type of statistics (coherent, Gaussian, or in between). Here the phonon degeneracy factor satisfies $N \gg 1$, and a classical approach is used. The phonon distribution function is known to be Gaussian in the equilibrium state; the same type of statistics is encountered in the thermal regime of the population of phonon modes. The scattering intensity increases abruptly (in comparison with the spontaneous process), simplifying the analysis of the characteristics of the scattered field, for example, the higher moments. The observed features of the angular line profile $g^{(2)}(\Delta \mathbf{k})$ fosters hope for the possibility of utilizing intensity fluctuation spectroscopy in the investigation of the properties of localized elementary excitations, for example, optical phonons and polaritons in spatially bounded media.

On the other hand, the choice of acoustic phonons ($\hbar\omega < kT$) — long-lived quasiparticles — as the scattered object is regarded as an intermediate case in passage from the limit of elastic scattering by permittivity fluctuations²⁰ to the limit of scattering by optical phonons, where $\hbar\omega \approx kT$. A further increase in the Raman frequency shift involves a change in the statistics of the scattered field, where the bunching parameter grows without bound.² The high contrast of the correlation functions in this case obviates the need for ultrafast photodetection systems ($\tau_{\text{eff}} < \tau_{\text{coh}} \approx 100$ ps) as in scattering by acoustic phonons. We can therefore approach a situation in which the light statistics changes from quantum (with high contrast on the part of the correlation functions) to classical thermal and coherent in a single scattering process.

This work received financial support from the Russian Fund for Fundamental Research (Grant No. 96-02-16334a).

¹⁾The instantaneous (i.e., averaged over a time of the order of τ_{coh}) intensity distribution, of course, contains the same information as the second-order intensity correlation functions.

¹B. Crosignani, P. Di Porto, and M. Bertolotti, *Statistical Properties of Scattered Light*, Academic Press, New York (1975).

²D. N. Klyshko, *Kvantovaya Élektron.* **4**, 1341 (1977) [*Sov. J. Quantum Electron.* **7**, 755 (1977)].

³A. V. Belinskii and M. V. Chekhova, *Zh. Éksp. Teor. Fiz.* **108**, 1956 (1995) [*JETP* **81**, 1067 (1995)].

⁴M. Artoni and J. L. Birman, *Phys. Rev. B* **44**, 3736 (1991).

⁵A. S. Shumovsky and B. Tanatar, *Phys. Rev. A* **182**, 411 (1993).

- ⁶E. Wolf, *Opt. Acta* **13**, 281 (1966).
- ⁷N. I. Lebedev, *Vestn. Mosk. Univ. Fiz. Astron.* **23**, 41 (1982).
- ⁸S. A. Akhmanov, Yu. E. D'yakov, and A. S. Chirkin, *Introduction to Statistical Radiophysics and Optics* [in Russian], Nauka, Moscow (1981).
- ⁹V. I. Balyakshii, V. N. Partygin, and L. E. Chirkov, *Physical Principles of Acoustooptics* [in Russian], Radio i Svyaz', Moscow (1985).
- ¹⁰W. Martienssen and E. Spiller, *Am. J. Phys.* **32**, 919 (1964).
- ¹¹E. Matieu and H. Keller, *J. Appl. Phys.* **41**, 1560 (1970).
- ¹²A. B. Haner and N. R. Isenor, *Am. J. Phys.* **38**, 748 (1970).
- ¹³V. G. Baryshevskii and M. I. Podgoretskii, *Zh. Éksp. Teor. Fiz.* **55**, 312 (1969) [*Sov. Phys. JETP* **28**, 165 (1969)].
- ¹⁴R. H. Brown and R. Q. Twiss, *Nature* **177**, 27 (1956); R. Q. Twiss, *Opt. Acta* **16**, 423 (1969).
- ¹⁵Z. Y. Ou, X. Y. Zou, L. J. Wang, and L. Mandel, *Phys. Rev. Lett.* **65**, 321 (1990).
- ¹⁶D. V. Strekalov, A. V. Sergienko, D. N. Klyshko, and Y. H. Shih, *Phys. Rev. Lett.* **74**, 3600 (1995).
- ¹⁷T. B. Pittman, Y. H. Shih, D. V. Strekalov, and A. V. Sergienko, *Phys. Rev. A* **52**, 3429 (1995).
- ¹⁸A. K. Ekert, J. G. Rarity, P. R. Tapster, and J. M. Palma, *Phys. Rev. Lett.* **69**, 1293 (1992).
- ¹⁹D. N. Klyshko, *Usp. Fiz. Nauk* **164**, 1187 (1994).
- ²⁰S. P. Kulik, A. N. Penin, and P. A. Prudkovskii, *Zh. Éksp. Teor. Fiz.* **106**, 993 (1994) [*JETP* **79**, 543 (1994)].

Translated by James S. Wood